

Automatic velocity analysis of crosswell seismic data

Guoping Li and Robert R. Stewart

ABSTRACT

A new method for velocity analysis of crosswell seismic data is discussed in this paper. Based on semblance analysis, this method derives velocities from crosswell direct arrivals in an automatic manner and so avoids time-consuming hand picking of traveltimes. To develop the method, an isotropic continuous elastic medium with a linear velocity-depth relationship is assumed. Two steps are involved. In the first step, traveltimes for direct arrivals are calculated for different velocity guesses, using theoretical equations we derive for a linear velocity function. Theoretically calculated traveltime trajectories of direct arrivals have been found to exhibit a quasi-hyperbolic pattern, one characteristic appearing on real crosswell data. A numerical study shows that they agree very well with those measured from synthetic data. In the second step, coherency (semblance) analysis is done for amplitudes of direct arrivals within a time window along each traveltime trajectory calculated for different velocity guesses. The velocity with the largest semblance value is then picked and used as final inversion output.

Examples of inverting velocity information from direct arrivals in synthetic, physical modeling, and field crosswell seismic data gathers, by using the new velocity analysis method, are given. Results prove this method to be a potential velocity inversion technique with efficiency and reliability.

INTRODUCTION

Crosswell seismic data are acquired by using two (or more) drilling wells: shooting the seismic source in one well, and recording the propagating waves in the other well offset by a certain distance. In crosswell surveys, seismic waves usually are generated and recorded below the highly attenuative near-surface zone and travel a relatively short distance between the wells, so high-fidelity data can be obtained. Therefore, compared to other seismic information sources (surface seismic or VSP), high resolution crosswell seismic data should provide more reliable information regarding subsurface physical parameters such as velocity.

For many years, attempts have been made to obtain velocity information from crosswell seismic data using tomographic inversion methods (Bois et al., 1972; Ivansson, 1985; Peterson et al., 1985; Bregman et al., 1989; Lines and LaFehr, 1989; Abdalla et al., 1990; Lines and Tan, 1990; Stewart, 1990). However, it has been recognized that most current tomographic techniques involve time-consuming hand picking of traveltimes. When hundreds of crosswell data gathers, for example, need to be analysed, hand-picking of traveltimes is not efficient.

In this paper, we will discuss a different crosswell velocity analysis method which makes use of the basic concept of coherency-based velocity analysis used for conventional surface seismic data. We assume that a linear velocity variation with depth is good enough to describe the intervening medium between wells. Traveltimes are calculated theoretically for crosswell direct arrivals for each velocity guess. Within a fixed time window along the calculated traveltime trajectory, seismic traces are scanned to find the best coherency (largest semblance value). The procedure is repeated until all possible velocity guesses are tried. As a result, the largest semblance value corresponds to the best-fit velocity. Since semblance analysis can be done automatically, the whole velocity analysis is done in an automatic manner, thus avoiding the process of hand-picking traveltimes which is required by traditional tomographic methods. In the following sections, we will discuss this automatic velocity analysis method in detail. Some examples of application to various crosswell seismic datasets will be given.

THEORY

Linear gradient medium

In seismic exploration, it is significant to make a proper assumption about the seismic wave velocity distribution in subsurface solid materials. Although adopted at times, the assumption of homogeneous isotropic media is a rough approximation to the actual earth. However, the concept of gradient medium, where velocity changes according to some simple mathematical function of distance from a reference plane, has been found more useful (Helbig, 1990). In such media, rays are curved everywhere, but are similar for all ray parameters. Moreover, wavefronts are of similar shapes for all traveltimes.

Particularly, a *linear-gradient medium* has been investigated by many geophysicists and found to be a very good approximation to the real solid earth. Slotnick (1959) wrote that the velocity of seismic wave propagation in Tertiary basins can be closely approximated by expressing it as linear function of depth. He gave some examples of areas, including the Gulf of Mexico, San Joaquin Valley of California, and a Venezuela basin, where 'one can safely assume a linear velocity relationship with depth'. Northwards, Jain (1987) finds, after inspecting sonic logs from western Canada, that most logs in the western Canadian basin justify a linear increase in velocity with depth down to the Paleozoic unconformity. The values of the velocity gradient he obtains from the Cretaceous section range from 0.25 to 1.0 ft/sec/ft.

A commonly-used expression for the linear velocity relation with depth is

$$V(Z) = V_0 + \kappa Z, \quad (1)$$

where V_0 is the initial velocity (ft/sec or m/sec), κ is the velocity gradient (ft/sec/ft, or m/sec/m, or 1/second), Z is depth (ft or m). The value of κ indicates an increase (when κ is positive) or decrease (when κ is negative) in velocity per unit of depth.

Sometimes the linear velocity function is expressed in the alternative form

$$V(Z) = V_0(1 + \eta Z) . \quad (2)$$

Here η is called velocity gradient factor, and its dimension is (feet)⁻¹ [or (meters)⁻¹]. Comparing equations (1) and (2), we have

$$\kappa = V_0\eta . \quad (3)$$

In this paper, relation (1) is used.

Traveltime equations for direct arrivals

In Appendix I, we have discussed some fundamental characteristics of propagation of crosswell direct waves in the isotropic elastic medium where the velocity function has the form of equation (1). In this kind of media, seismic waves propagate along circular raypaths whose radii and centers are closely related to velocity parameters.

Also in Appendix I, we have derived expressions for direct arrival traveltimes, namely, equation (A-I-4b) and equation (A-I-11b). In fact, they are equivalent except for the difference in sign. So we can write them into a combined form since traveltime is always positive:

$$t = \frac{1}{\kappa} \left| \ln \frac{(V_0 + \kappa Z) (\sqrt{1 - p^2(V_0 + \kappa Z_S)^2 + 1})}{(V_0 + \kappa Z_S) (\sqrt{1 - p^2(V_0 + \kappa Z)^2 + 1})} \right| . \quad (4)$$

where t - traveltime for direct arrivals;
 Z - depth of the receiver;
 Z_S - depth of the source; and
 p - ray parameter.

To calculate traveltimes, we need to know the unknown parameter p in equation (4). We have known that the paths of direct seismic waves, traveling in a linear velocity gradient medium between the recording well and the source well, are circular arcs. Therefore they must satisfy the equation for a circle. Mathematically, two points (a pair of source and receiver positions) cannot determine a circle uniquely and sufficiently. But it is known from Appendix I that the vertical coordinate of the center of a circular raypath is a constant determined by given velocity parameters. Then for some circular ray connecting the source point (X_S, Z_S) and the receiver point (X_R, Z_R) , we have

$$(X_S - X_C)^2 + (Z_S - Z_C)^2 = R^2 , \quad (5a)$$

$$(X_R - X_C)^2 + (Z_R - Z_C)^2 = R^2 , \quad (5b)$$

where X_C, Z_C - center of the circular arc; and
 R - radius of the circular arc.

Solving (5) gives

$$X_C = \frac{X_R^2 - X_S^2 + (Z_R - Z_C)^2 - (Z_S - Z_C)^2}{2(X_R - X_S)} , \quad (6a)$$

and

$$R = \sqrt{(X_S - X_C)^2 + (Z_S - Z_C)^2} \quad (6b)$$

Therefore the ray parameter p for this particular circular locus is given by

$$p = \frac{1}{R\kappa} \quad (7)$$

With the parameter p determined, we are now able to calculate the traveltimes from the source to the receiver.

The discussion in Appendix I tells us that if the initial emission angle of the ray $\alpha_0 < 90^\circ$, we need to take into account the effect of diving waves on traveltimes. One method (as used by Slotnick, 1959) is to find the deepest ray penetration point and do the traveltimes integration from the source position to this point and then from this point to the receiver position. The deepest penetration point can be readily found by setting $X = X_C$ in equation (A-I-5), which gives

$$Z_{\max} = \frac{1}{\kappa p} - \frac{V_0}{\kappa} = R - \frac{V_0}{\kappa} \quad (8)$$

Now, the traveltimes can be calculated via

$$\begin{aligned} t &= \int_{Z_S}^{Z_{\max}} \frac{dz}{(V_0 + \kappa Z) \sqrt{1 - \left(\frac{V_0 + \kappa Z}{R\kappa}\right)^2}} - \int_{Z_{\max}}^{Z_R} \frac{dz}{(V_0 + \kappa Z) \sqrt{1 - \left(\frac{V_0 + \kappa Z}{R\kappa}\right)^2}} \\ &= \frac{1}{\kappa} \ln \frac{(V_0 + \kappa Z_{\max}) \left(\sqrt{1 - \left(\frac{V_0 + \kappa Z_S}{R\kappa}\right)^2} + 1 \right)}{(V_0 + \kappa Z_S) \left(\sqrt{1 - \left(\frac{V_0 + \kappa Z_{\max}}{R\kappa}\right)^2} + 1 \right)} \\ &\quad + \frac{1}{\kappa} \ln \frac{(V_0 + \kappa Z_{\max}) \left(\sqrt{1 - \left(\frac{V_0 + \kappa Z_R}{R\kappa}\right)^2} + 1 \right)}{(V_0 + \kappa Z_R) \left(\sqrt{1 - \left(\frac{V_0 + \kappa Z_{\max}}{R\kappa}\right)^2} + 1 \right)} \quad (9) \end{aligned}$$

Substituting equation (8), the above equation is reduced to

$$t = \frac{1}{\kappa} \ln \frac{R\kappa \left(\sqrt{1 - \left(\frac{V_0 + \kappa Z_S}{R\kappa}\right)^2} + 1 \right)}{(V_0 + \kappa Z_S)} + \frac{1}{\kappa} \ln \frac{R\kappa \left(\sqrt{1 - \left(\frac{V_0 + \kappa Z_R}{R\kappa}\right)^2} + 1 \right)}{(V_0 + \kappa Z_R)} \quad (10)$$

When $Z_R = Z_S$, we have

$$t = \frac{2}{\kappa} \ln \frac{R\kappa \left(\sqrt{1 - \left(\frac{V_0 + \kappa Z_S}{R\kappa} \right)^2} + 1 \right)}{(V_0 + \kappa Z_S)} . \quad (11)$$

Slotnick (1959) and Grant and West (1965) obtained the same result for the case of $Z_R = Z_S = 0$.

The method to determine when equation (4) or (10) should be used to calculate traveltimes is to know the depth at which the ray would leave the source at a 90° angle. This depth can be easily found. In crosswell seismic surveys, the separation distance between the wells, X , is usually fixed, and $X = X_R - X_S$ (in the vertical borehole case). For $\alpha_o = 90^\circ$, $p = 1/(V_0 + \kappa Z_S)$. Then from equation (A-I-5) or (A-I-12), we have

$$X^2 + \left(Z + \frac{V_0}{\kappa} \right)^2 = \left(\frac{V_0 + \kappa Z_S}{\kappa} \right)^2 , \quad (12)$$

which gives one solution

$$Z_1 = \sqrt{\left(\frac{V_0 + \kappa Z_S}{\kappa} \right)^2 - X^2} - \frac{V_0}{\kappa} . \quad (13)$$

Now, if the receiver depth Z_R is less than or equal to Z_1 , then equation (4) should be used. If $Z_1 < Z_R$ and $X_C < X$, then equation (10) ought to be used. But if $Z_1 < Z_R \leq Z_{max}$ and $X_C \geq X$, equation (4) is used.

It is found that equations (4) and (10) actually can be combined together into a single but more concise formula (Baerg, 1991):

$$t = \frac{1}{\kappa} \ln \left(\frac{Z_R - Z_C}{Z_S - Z_C} \frac{R + X_C - X_S}{R + X_C - X_R} \right) . \quad (14)$$

VELOCITY ANALYSIS METHOD

It has been known from the above discussion that once crosswell geometry parameters (source position, receiver position, and well separation) are given, and parameters in the linear velocity function (initial velocity and gradient) are known, traveltimes of direct arrivals can be theoretically calculated for all source-receiver pairs. These traveltimes define a quasi-hyperbolic trajectory, as will be seen later on. For a particular crosswell data gather where the geometry is known, keeping the two velocity parameters changing respectively will lead to different traveltime trajectories, among which one may best fit the observed direct arrival event. Now the question is, if we can approximate the direct arrival event of real crosswell data with a theoretical trajectory, can we obtain an approximate velocity distribution? Our crosswell velocity analysis method, based upon automatic semblance scanning, is trying to answer this question.

The automatic velocity analysis method comprises two steps. In the first step, direct arrival traveltimes are calculated at all receiver (or source) positions in a given crosswell geometry, using equations (4) and (10), or equation (14). All possible velocity guesses are tried, resulting in a set of traveltime curves (trajectories). Then in the second step, seismic traces in a crosswell data gather are scanned within a time window along each traveltime trajectory calculated in the first step. Based on this, semblance analysis is then conducted.

Semblance analysis

A useful measure of coherency of signals is their energy. According to Yilmaz (1987) and Krebs (1989), the output energy is defined as

$$E_{\text{out}} = \sum_{t=t(i)-\Delta t}^{t(i)+\Delta t} \left(\sum_{i=1}^N f_{i,t} \right)^2, \quad (15)$$

and the input energy as

$$E_{\text{in}} = \sum_{t=t(i)-\Delta t}^{t(i)+\Delta t} \left(\sum_{i=1}^N f_{i,t}^2 \right), \quad (16)$$

where

- i - the i^{th} seismic trace;
- $t(i)$ - the traveltime corresponding to the i^{th} trace;
- $f_{i,t}$ - the amplitude of the i^{th} trace at time $t(i)$ within window $[-\Delta t, \Delta t]$; and
- N - the total number of traces involved.

Therefore, the semblance value can be found from

$$S_c = \frac{E_{\text{out}}}{N E_{\text{in}}}, \quad 0 \leq S_c \leq 1. \quad (17)$$

The semblance value provides a criterion for determining whether or not the theoretically derived traveltime curve best fits the direct arrival trajectory of the real data, and further determining whether or not the velocity function being used is the best one. The larger the semblance value, the more coherent the direct arrival event of the data that has been scanned, and therefore, the better the velocity function. Accordingly, velocity parameters that give the largest semblance value is selected.

Algorithm implementation

The algorithm has been implemented with a computer program operatable on workstations or personal computers. Shown in Figure 1 is the computation procedure, which is composed of the following parts:

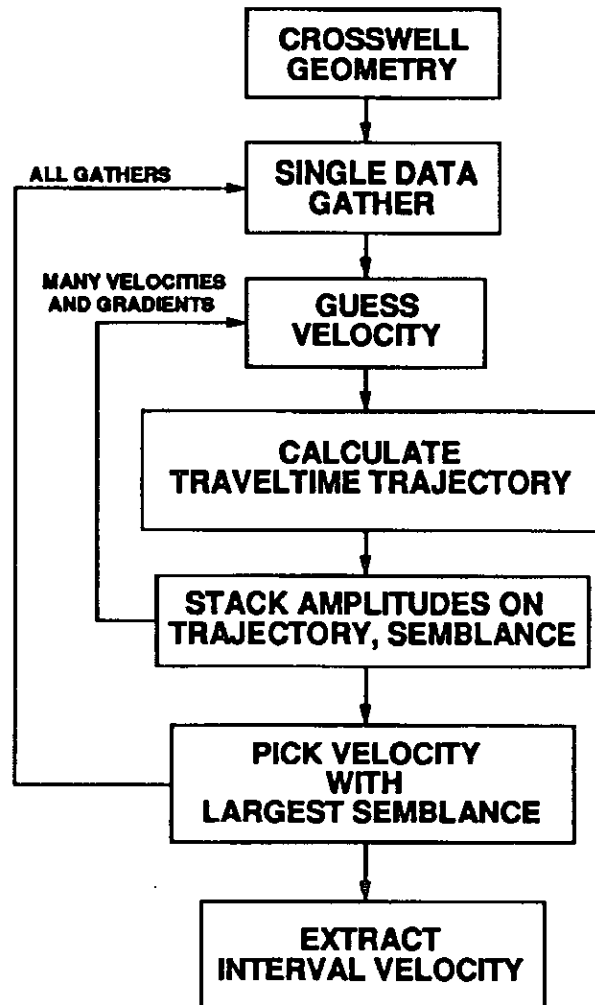


FIG. 1. Processing procedure for automatic velocity analysis of crosswell seismic data.

- . Enter crosswell geometry;
- . Input a crosswell data gather (common source or common receiver);
- . Scan through a range of κ and V_0 values;
 - Calculate traveltime, $t(i)$, for every trace;
 - Stack the trace amplitudes along the calculated traveltime trajectory, within a given time window $[-\Delta t, \Delta t]$;
 - Calculate semblance value;
- . Pick the velocity which corresponds to the largest semblance value;
- . Do this whole procedure for next gather from a different depth aperture, and find a new velocity function; until all gathers are processed.

- . Extract the final interval velocity distribution by fitting all velocity functions obtained from different depth apertures.

TESTING

The automatic crosswell velocity analysis method has been tested with different data sets. In this paper, we give some examples of applying this method to synthetic data, physical modeling data, and a field crosswell data gather.

Synthetic data

Synthetic crosswell seismic data used to test our method were generated with the UNISEIS ray tracing program. The geologic model we used is shown in Figure 2. It is composed of 71 horizontal layers with equal thickness (20 m) in each layer. Velocity distribution in this multiple layered model obeys a linear velocity-depth relationship as follows

$$V = 2000 + 0.8Z \quad (\text{m/s}), \quad (18)$$

but in individual layers, velocities are constant and take the value calculated using (18) in the middle of each layer.

To record crosswell seismic data, source and receivers were positioned respectively on the two sides of the model, which were separated 500 m. Receiver depths ranged from 0 m to 1200 m. Common shot gathers were collected when the source was 'excited' at different depths. Shot gathers contain 121 seismic traces each. Only rays for direct arrivals were traced for our purpose. During ray tracing, the source was fired at depths of 0 m, 260 m, 500 m, 760 m, and 1000 m, separately. To generate crosswell sections, zero-phase Ricker wavelets were used. The wavelets were 60 ms long and had a center frequency of 40 Hz. Shown in Figures (3) and (4) are two shot gathers corresponding to the source depths of 0 m and 500 m, respectively. Direct arrivals are displayed clearly in both figures.

To test precision of the traveltimes equations we derived, theoretical traveltimes were calculated for one common shot gathers (source depth is 500 m), using equations (4) and (10). Their comparison with traveltimes measured on the synthetic section (Figure 4) is given in Figure 5. It can be seen from Figure 4 or Figure 5(a) that the traveltime curve has a quasi-hyperbolic shape, which is observable on real crosswell data. Figure 5(b) reveals that the difference between the theoretical and the traced traveltimes is very small (the maximum absolute differential time is about 3 ms), indicating that our traveltime equations provide sufficient precision. It implies that if correct velocity is used, traveltime trajectory of real crosswell data can be approximated with high precision. This provides the basis for automatic velocity analysis.

To run the automatic velocity analysis program, crosswell parameters for a shot gather must be provided. A wide range of initial velocities and of velocity gradients is scanned for the best selection which agrees with the largest semblance value.

For the synthetic data in hand, we scanned for the best velocity from 1900 m/s to 2100 m/s (at interval of 10 m/s) and for the best gradient from 0.5 m/s/m to 1.1 m/s/m (at

interval of 0.05 m/s/m). A time window equal to the length of the Ricker wavelet used was opened for semblance analysis. The results of semblance analysis were finally contoured for the ease of picking the largest values. Figure 6 shows the result of semblance analysis for the shot gather for source depth of 0 m. The largest semblance value appears at the point where the initial velocity is 2000 m/s and velocity gradient is 0.8 m/s/m. The inversion method has reconstructed the velocity function used to generate the geologic model. The same results are obtained from semblance analysis of shot gathers corresponding to source depths of 500 m (Figure 7), and 760 m (Figure 8). Thus, velocity distribution in a layered model can be confidently recovered by applying the automatic velocity analysis method to crosswell data.

However, small errors in velocity analysis are also noted. Figure 9 shows the semblance analysis result for the gather with the source 260 m deep. Largest semblance value is obtained when initial velocity is 2010 m/s and gradient is 0.8 m/s/m. Figure 10 shows the semblance analysis result for the data gather at the source depth of 1000 m. At the point at which the initial velocity is 1990 m/s and the gradient is 0.825 m/s/m, there exists the largest semblance value. Thus, the final inversion results from analysis of these two gathers have a shift, but very small, from the actual velocity function.

Physical modeling data

Physical modeling data were from an ultrasonic borehole seismic modeling experiment accomplished at the University of Calgary (Stewart and Cheadle, 1989). 40 crosswell shot gathers, each having 40 traces, were collected in a geometry where ultrasonic source and receiver transducers were deployed along the two sides of a target model (a Teflon cylinder 3.81 cm) located in water tank. Source spacing and receiver spacing were 50 m, and the well separation was 600 m, in a scaled distance. Two shot records with the source shot at 0 m and 1000 m are shown in Figure 11. Note that the direct arrivals at several traces in the middle of Figure 11(b) are pulled down because of the velocity of the Teflon model lower than that of the surrounding water.

The automatic velocity analysis method was applied to three gathers for source depths of 0 m, 450 m, and 1000 m, respectively, in order to see whether or not the background velocity (that is, water velocity which is around 1490 m/s) can be inverted from direct arrivals. The guessed initial velocities ranged from 1000 m/s to 1800 m/s at interval of 20 m/s. The velocity gradient was guessed between 0.00001 m/s/m and 0.01 m/s/m. The length of the wavelet, which was used as width of the time window for velocity analysis, was 30 ms.

Figures 12-14 show the results of semblance analysis for the gathers from different source positions. In Figure 12, the best velocity should be picked from where the initial velocity is 1520 m/s and gradient is 0.0095 m/s/m. In Figure 13, the best inverted velocity is formed by the initial velocity of 1520 m/s and the gradient of 0.0085 m/s/m. Figure 14 shows that the largest semblance value corresponding to the initial velocity of 1520 m/s and velocity gradient of 0.0065 m/s/m gives the best selection for velocity. From the above results, the initial velocity inverted is consistently 1520 m/s, with a 2.0% difference in value from the real velocity of 1490 m/s. The gradient value obtained from the velocity analysis change from 0.0065 m/s/m to 0.0095 m/s/m, causing velocity variation by 13 ~ 19 m/s within the depth aperture of 2000 m. Thus, the velocity changes caused by the velocity gradient is negligible. In short, the velocity inverted from the physical modeling crosswell data using our method is very close to the actual model velocity.

Field data

The real crosswell seismic data were acquired in Humble, Texas (courtesy of Texaco Inc.). In Figure 15, a common-receiver gather is shown, which is composed of 113 traces, representing a depth aperture of 300 ft (91.5 m) to 2540 ft (774.4 m). The receiver was at the depth of 1500 ft (457.3 m). Well-to-well separation was 815 ft (248.5 m). Seismic traces were recorded at sample interval of 0.25 ms. P-wave direct arrivals, denoted with the letter *D*, has a quasi-hyperbolic travelttime trajectory, as mentioned before. The hyperbolic trajectory is not symmetric partly because of variations of velocity in the subsurface, and partly because of crosswell recording geometry. It can be seen in Figure 15 that the data contain very strong tube wave energy, which dominates the record.

The automatic velocity analysis program searches for the optimal velocity in that particular depth aperture by scanning velocity in a range of 4900 ft/sec to 16500 ft/sec (interval 200 ft/sec) and gradient in a range of 0.045 ft/sec/ft to 2.0 ft/sec/ft (interval 0.1 ft/sec/ft). Time window of 14 ms wide (approximately wavelet width) was used to scan seismic traces around direct arrivals. Figure 16 is the result of velocity analysis. Velocity is picked at the initial velocity of 6100 ft/sec and gradient of 0.145 ft/sec. From the new velocity function, velocity changes from 6143.5 ft/sec to 6468.3 ft/sec in an aperture from 300 ft to 2540 ft. Although unfortunately we currently do not have other velocity information in this area to confirm the inverted velocity function, velocities we have shown appear to be reasonable.

DISCUSSION

The inversion problem may not be unique. For example, in Figures 6, 9, and 10, there are several local highs within a narrow belt in the semblance map. These local highs have values very close to the one that we picked, making interpretation difficult. This problem arises because combinations of smaller initial velocity and larger gradient or of larger initial velocity and smaller gradient may generate the same effect as does the combination of the correct initial velocity and gradient. Therefore, precaution must be taken in interpreting the inversion results. Fortunately, in our case, the semblance value which gave the inverted velocity is after all larger than these highs around it.

Problems may also be caused when the available crosswell data are noisy. Noise has an obvious effect on the results of semblance analysis because in addition to signals, noise within the given time window is also involved in calculation of semblance values [see equations (15) and (16)]. Thus, application of band-pass filters to crosswell seismic data, prior to velocity analysis, is recommended. It is also found that inversion result will be good if the width of time window is close to the wavelet length. It will be useful to apply a wavelet shaping process to real data to make wavelets consistent from trace to trace.

In this paper, we did not discuss the case of negative velocity gradient, a case that may exist in some areas. But as we can see, it is not difficult to generalize our discussion. The basic idea we have developed here still applies, except for some modifications in travelttime equations we derived previously. Mathematically, it is not difficult either to generalize our discussion to the case of deviated wells. This velocity analysis method can also be applied to S-wave crosswell data.

CONCLUSIONS

It is possible now to automatically derive velocity from crosswell seismic data, in a simple but efficient way with the velocity analysis method we have discussed in this paper. Without having to pick traveltimes by hand, this method estimates a velocity distribution from crosswell direct arrivals by conducting an automatic semblance analysis for seismic traces around traveltimes of direct arrivals theoretically calculated, assuming a linear velocity-depth relationship. This method has been tested on a number of crosswell data gathers. Inversion results are satisfactory.

FUTURE WORK

The automatic crosswell velocity analysis method discussed here has shown an exceptionally encouraging perspective. But as this method is still in the early stage, more research is required to improve it.

It is not unusual that in some areas, the subsurface velocity is distributed with several velocity gradients within different depths. Such multiple gradients in the same area would cause the direct arrivals to behave differently than what we have dealt with before. In this situation, direct arrival events may no longer be described by the smooth quasi-hyperbolic trajectory which is obtained from our traveltime equations. Therefore, in such cases, multi-scan may be necessary. That is, the entire depth aperture of interest may need to be divided into a number of sub-apertures, within each of which, velocity analysis is conducted using our method. Inversion results from these sub-apertures are finally combined together.

Besides, it is worth investigating other velocity-depth functions, which may be more accurate and more suitable to describe subsurface velocity patterns than the linear one we have used in this paper.

Since random or coherent noise has a strong influence on the result of semblance analysis, we may not always be able to obtain reliable velocity inversion results. Thus, some noise-resistant coherency measures may need to be considered.

ACKNOWLEDGEMENTS

We are very grateful for technical help and valuable suggestions of M. Harrison, H. Bland, D. Easley, Dr. D. Lawton, T. Howell, E. Gallant, S. Miller, J. Baerg and Y. Song, during this research. The generous donation of real crosswell seismic data by Texaco Inc. (USA) is sincerely acknowledged. We also wish to thank all sponsors of the CREWES Project for their continuous support. This research was supported by the CREWES Project.

REFERENCES

- Abdalla, A.A., Stewart, R.R., and Henley, D.C., 1990, Reflection processing of crosswell seismic data: Midale field, Saskatchewan: CREWES Project Research Report, The University of Calgary, Vol. 2, 225-259.
- Baerg, J.R., 1985, Analysis of cocrust seismic refraction and wide angle reflection experiments from southern Saskatchewan and Manitoba: M.Sc. thesis, The University of Western Ontario.
- Baerg, J.R., 1991, Traveltime in media with linear velocity-depth functions: this volume.
- Bois, P., La Porte, M., Lavergne, M., and Thomas, G., 1972, Well-to-well seismic measurements: *Geophysics*, **37**, 471-480.
- Bregman, N.D., Bailey, R.C., and Chapman, C.H., 1989, Crosshole seismic tomography: *Geophysics*, **54**, 200-215.
- Grant, F.S., and West, G.F., 1965, Interpretation theory in applied geophysics: McGraw-Hill Book Company, New York.
- Helbig, K., 1990, Rays and wavefront charts in gradient media: *Geophysical Prospecting*, **38**, 189-220.
- Ivansson S., 1985, A study of methods for tomographic velocity estimation in the presence of low-velocity zones: *Geophysics*, **50**, 969-988.
- Jain, S., 1987, Amplitude-vs-offset analysis: A review with reference to application in western Canada: *J. Can. Soc. Expl. Geophys.* **23**, No. 1.
- Krebes, E.S., 1989, Geophysical data processing: Course Notes, The University of Calgary.
- Lines, L., and Tan, H., 1990, Cross-borehole analysis of velocity and density: Expanded Abstracts, 1990 SEG meeting, San Francisco.
- Lines, L.R., and LaFehr, E.D., 1989, Tomographic modeling of a cross-borehole data set: *Geophysics*, **54**, 1249-1257.
- Peterson, J.E., Paulsson, B.N.P., and McEvelly, T.V., 1985, Applications of algebraic reconstruction techniques to crosshole seismic data: *Geophysics*, **50**, 1566-1580.
- Slotnick, M.M., 1959, Lessons in seismic computing, Ed. by Geyer R.A., Society of Exploration Geophysicists.
- Stewart, R.R., 1990, Exploration seismic tomography: Fundamentals: Continuing Education Course Notes, Society of Exploration Geophysicists.
- Stewart, R.R., and Cheadle, S.P., 1989, Ultrasonic modeling of borehole seismic surveys: CREWES Project Research Report, The University of Calgary, Vol. 1, 206 - 224.
- Telford, W.M., Geldart, L.P., Sheriff, R.E., and Keys, D.A., 1976, Applied Geophysics: Cambridge University Press.
- Yilmaz, O., 1987, Seismic data processing: Society of Exploration Geophysicists.

APPENDIX I

WAVE PROPAGATION IN A LINEAR GRADIENT MEDIUM

In this section, we will examine some fundamental characteristics of seismic wave propagation in a linear velocity-gradient medium. Because we concern ourselves mainly with applications to crosswell seismic data, we choose to consider the crosswell surveying geometry. In addition, for our purpose, we consider direct arrivals only. Therefore, relevant expressions for raypaths and traveltimes of direct waves will be derived.

Let us first establish a Cartesian coordinate system such that the X-axis is on the flat surface of the earth, the Z-axis is along the symmetrical axis of a vertical borehole, and the origin of the coordinate system is at the wellhead. Suppose that the source S is at $(0, Z_s)$, where $Z_s \geq 0$, and an arbitrary point R is at (X, Z) . A seismic wave leaves the source S at

the angle α_0 to the vertical axis, and travels to R along a curved raypath \widehat{SR} . The geometry is shown in Figure A-I-1.

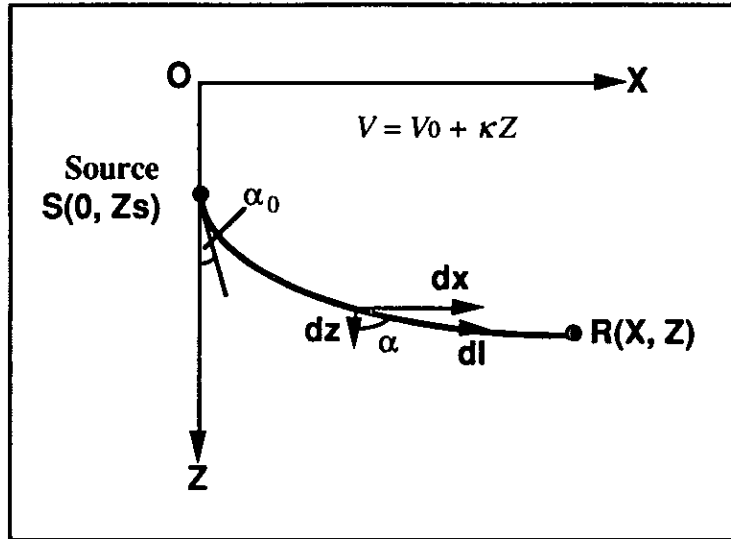


FIG. A-I-1. Geometry showing a seismic ray leaving the source and propagating in a continuous medium.

The energy generated by the seismic source will radiate outwards in all directions. In crosswell surveying geometries, angles of the rays emitted from the source range between 0° and 180° . When the emission angle α_0 is 90° , the ray leaves the source horizontally, and then gradually turns upward. However, when the angle is less than 90° , diving waves would be expected to occur. Therefore, it is necessary to discuss two cases:

- 1) $\alpha_0 \leq 90^\circ$; and 2) $\alpha_0 > 90^\circ$.

Case I: Ray emission angle not larger than 90°

This is the case in which the seismic wave, upon leaving the source, travels downward into the medium below the source, or in a special situation when the angle of emission is 90° , it leaves the source horizontally and then travels upward. Let us look at an infinitesimal segment of the ray, dl (see Figure A-I-1). It makes an angle α with the vertical axis. We assume that all positive angles are measured counterclockwise from the vertical axis. This segment has a vertical component of dz and a horizontal component of dx . The following relations can be found:

$$\frac{dx}{dz} = \tan\alpha, \quad dl = \frac{dz}{\sqrt{1 - (\sin\alpha)^2}}, \quad dt = \frac{dl}{V}. \quad (\text{A-I-1})$$

The velocity V and the depth-dependent angle α are related by Snell's law:

$$p = \frac{\sin\alpha}{V}, \quad (\text{A-I-2})$$

which is the law governing wave propagation along a least-time path. Here, the ray parameter p is a constant which depends upon the direction in which the ray left the source, that is, upon the angle α_0 . By integrating equation (A-I-1) and substituting equation (A-I-2), we get two integral equations for the total horizontal distance X , and total traveltime t :

$$X = \int_{Z_s}^Z \frac{pVdz}{\sqrt{1 - p^2V^2}}, \quad (\text{A-I-3a})$$

$$t = \int_{Z_s}^Z \frac{dz}{V\sqrt{1 - p^2V^2}}. \quad (\text{A-I-3b})$$

Clearly, equation (A-I-3a) describes a family of curved raypaths, characterized by the corresponding values of the ray parameter p . Since p affects the raypaths, the traveltimes given by (A-I-3b) differ from one path to another. The assumption of linear velocity gradient, that is, equation (1) in the text body, leads to solutions of the above integrals:

$$X = \frac{1}{\kappa p} \left(\sqrt{1 - p^2(V_0 + \kappa Z_s)^2} - \sqrt{1 - p^2(V_0 + \kappa Z)^2} \right), \quad (\text{A-I-4a})$$

$$t = \frac{1}{\kappa} \ln \frac{(V_0 + \kappa Z) \left(\sqrt{1 - p^2(V_0 + \kappa Z_s)^2} + 1 \right)}{(V_0 + \kappa Z_s) \left(\sqrt{1 - p^2(V_0 + \kappa Z)^2} + 1 \right)}. \quad (\text{A-I-4b})$$

The solutions (A-I-4a) and (A-I-4b) can also be expressed in a different approach (Telford et al., 1976; Baerg, 1985).

The raypath given by equation (A-I-4a) is a circle in the X - Z plane; this can be shown by rearranging terms in equation (A-I-4a):

$$\left[X - \frac{\sqrt{1 - p^2(V_0 + \kappa Z_s)^2}}{\kappa p} \right]^2 + \left(Z + \frac{V_0}{\kappa} \right)^2 = \frac{1}{\kappa^2 p^2}. \quad (\text{A-I-5})$$

The center of the circular raypath is at $C(X_c, Z_c)$, where

$$X_c = \frac{\sqrt{1 - p^2(V_0 + \kappa Z_s)^2}}{\kappa p}, \quad (\text{A-I-6a})$$

$$Z_c = -\frac{V_0}{\kappa}, \quad (\text{A-I-6b})$$

and the radius R is

$$R = \frac{1}{\kappa p} \quad . \quad (A-I-7)$$

Therefore, in a linear velocity-gradient medium, seismic waves travel along circular raypaths, characterized by equation (A-I-5). Figure A-I-2 shows a seismic ray leaving the source at the angle α_0 and traveling along a circular path. The center, C , of the circular ray lies above the earth's surface a distance V_0/κ .

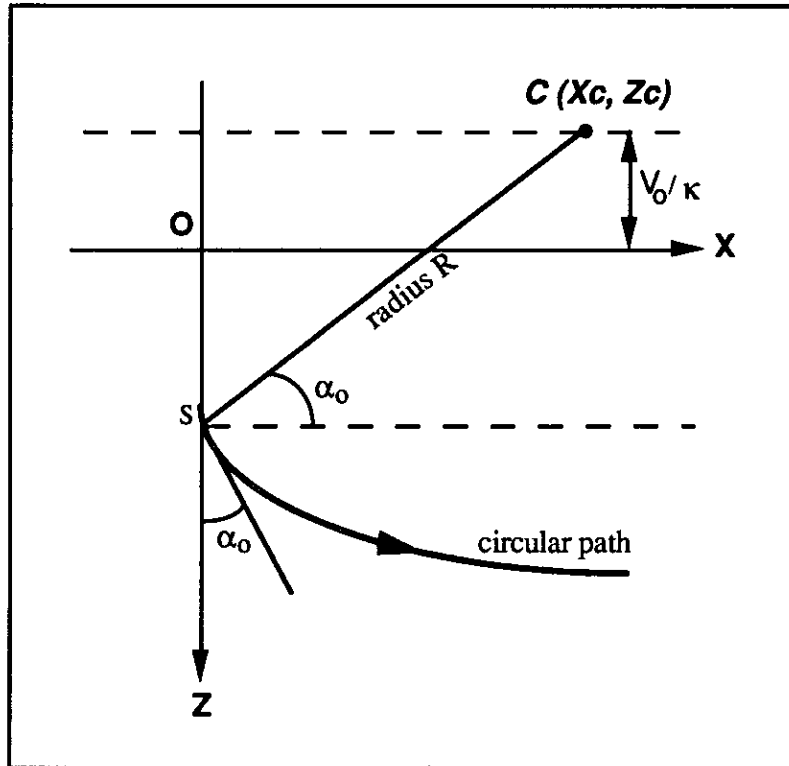


FIG. A-I-2. Circular raypath leaving the source S at the angle α_0 .

We find, in equation (A-I-6b), that the vertical coordinate of the center, Z_c , is independent of α_0 . The value of Z_c is determined by a given velocity function alone and thus is a constant. This means that the centers of all circular rays lie on the same horizontal line. This line is located where the velocity would be zero if the velocity function were extrapolated up to an elevation where $Z = -V_0/\kappa$ (Telford et al., 1976).

Furthermore, since parameters V_0 and κ , and ray parameter p , are given positive, the centers of those rays are all located within the $(+X, -Z)$ quadrant of the coordinate system. Equation (A-I-7) indicates that the radius of the circular ray depends upon the ray parameter p . Figure A-I-3 shows schematically some of the circular raypaths whose radii are different.

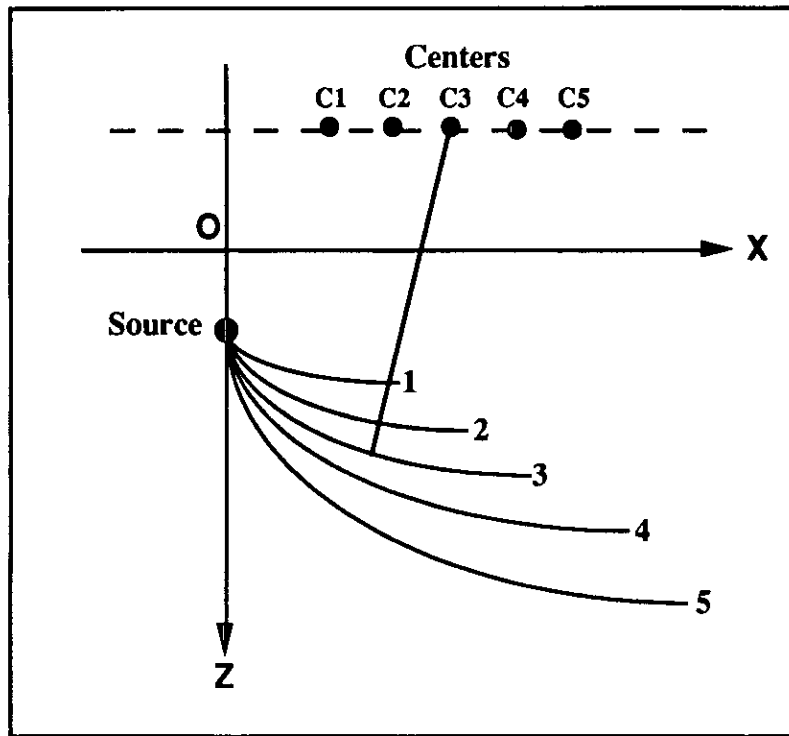


FIG. A-I-3. Circular raypaths with different radii and their centers.

From equation (A-I-6a), we can see that the horizontal coordinates of the centers of the circular rays are determined by non-negative values of Xc . In particular, when the emission angle $\alpha_0=90^\circ$, the raypath is such a circle whose center is at $(0, Zc)$. This can be shown by substituting

$$p = \frac{\sin\alpha_0}{V_0 + \kappa Zs} = \frac{\sin 90^\circ}{V_0 + \kappa Zs} = \frac{1}{V_0 + \kappa Zs}, \quad (\text{A-I-8})$$

into equation (A-I-6a). This situation is shown in Figure A-I-4. We see that at this time, no effect of diving waves (or turning waves, Grant and West, 1965) occurs.

From Figure A-I-4, it can be predicted that when $\alpha_0 > 90^\circ$, the centers of rays will be moved into the $(-X, -Z)$ quadrant of the coordinate system. This will be discussed in the next section.

Case II: Ray emission angle larger than 90°

In this case, the wave travels upward along a curved raypath as shown in Figure A-I-5. Let us discuss this situation and derive formulae for the raypath and traveltime. The derivation can be accomplished in a similar approach that we have used before. But note

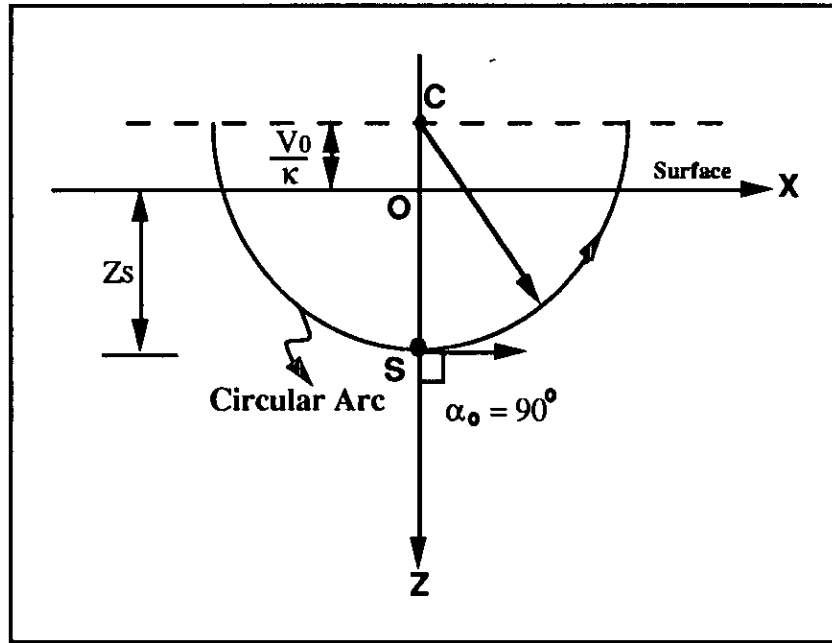


FIG. A-I-4. When the emission angle of the ray is 90° , the center of the circular raypath is on the vertical axis.

that the ray's angle α , in this case, is always greater than 90° . From Figure A-I-5, we see that

$$\theta = \alpha - 90^\circ, \quad (\text{A-I-9})$$

therefore,

$$\frac{dx}{dz} = \cotan\theta = \cotan(\alpha - 90^\circ) = -\tan\alpha = -\frac{\sin\alpha}{\sqrt{1 - (\sin\alpha)^2}}, \quad (\text{A-I-10a})$$

$$dt = \frac{dl}{V} = \frac{\sqrt{(dx)^2 + (dz)^2}}{V}. \quad (\text{A-I-10b})$$

Applying Snell's law (A-I-2) and the linear velocity function (Eq.1), and integrating equations (A-I-10a) and (A-I-10b) result in the following relations:

$$X = \frac{1}{\kappa p} \left(\sqrt{1 - p^2(V_0 + \kappa Z)^2} - \sqrt{1 - p^2(V_0 + \kappa Z_s)^2} \right), \quad (\text{A-I-11a})$$

$$t = \frac{1}{\kappa} \ln \frac{(V_0 + \kappa Z_s) \left(\sqrt{1 - p^2(V_0 + \kappa Z)^2} + 1 \right)}{(V_0 + \kappa Z) \left(\sqrt{1 - p^2(V_0 + \kappa Z_s)^2} + 1 \right)}. \quad (\text{A-I-11b})$$

Rearranging the terms in equation (A-I-11a), we have

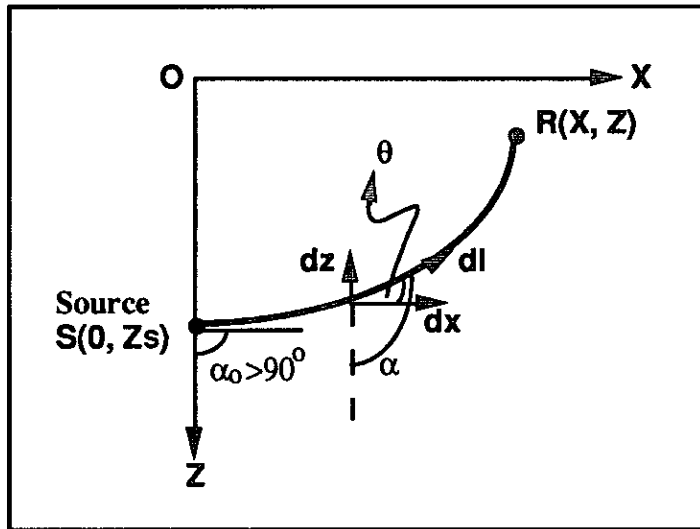


FIG. A-I-5. Geometry showing a seismic ray leaving the source and traveling upward in a continuous medium.

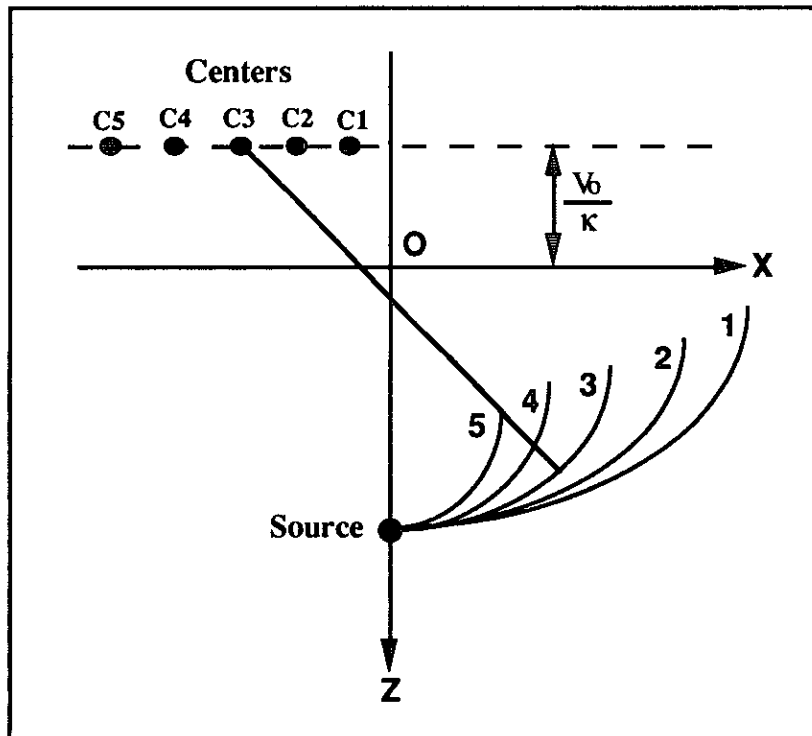


FIG. A-I-6. Circular raypaths and their centers.

$$\left[X + \frac{\sqrt{1 - p^2(V_0 + \kappa Z_s)^2}}{\kappa p} \right]^2 + \left(Z + \frac{V_0}{\kappa} \right)^2 = \frac{1}{\kappa^2 p^2} . \quad (\text{A-I-12})$$

Equation (A-I-12) tells us that the resulting raypath is a circular arc, whose center and radius are, respectively,

$$\text{Center at: } C \left(-\frac{\sqrt{1 - p^2(V_0 + \kappa Z_s)^2}}{\kappa p}, -\frac{V_0}{\kappa} \right) ,$$

and

$$\text{Radius: } R = \frac{1}{\kappa p} .$$

As can be seen, when the velocity gradient $\kappa > 0$, the center of the circular path is always located within the coordinate quadrant $(-X, -Z)$. The vertical coordinate of the center is independent of the ray parameter p while the radius varies with it. Again, the centers of all possible rays lie on the same horizontal line above the X -axis (the earth's surface) a certain distance. Figure A-I-6 shows some raypaths and their center positions.

In summary, seismic waves propagate along circular raypaths in a medium of a velocity increasing linearly with depth. The radii of these circular rays are inversely proportional to the product of the ray parameter p and the given velocity gradient κ . All the centers of these rays lie on the same line which is above the surface of the earth a distance determined by the two parameters of the given velocity function. When the emission angle α_0 , at which seismic rays leave the source position, is greater than 90° , rays travel upward and the centers of circles are located within the $(-X, -Z)$ zone. When $\alpha_0 < 90^\circ$, rays travel downward and then turn upward along those circular paths whose centers are within the $(+X, -Z)$ zone. In this case, the effect of diving waves occurs. When $\alpha_0 = 90^\circ$, there is only one ray that travels horizontally first and then bend upward. The center of this ray is located on the vertical axis of the coordinate system.

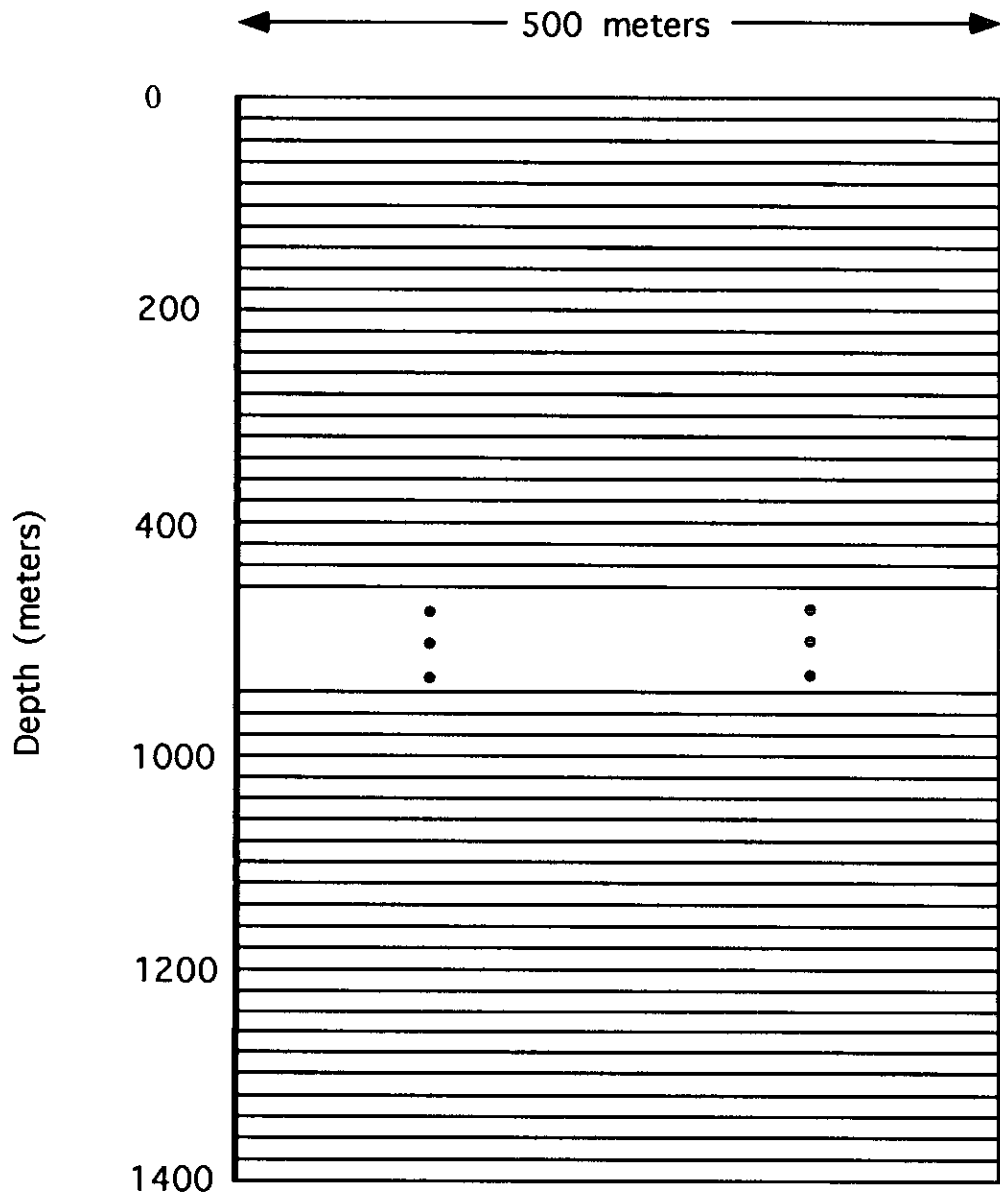


FIG. 2. Layered model used to generate synthetic crosswell seismic data. Each layer has the same thickness. Velocities in all layers satisfy a linear velocity-depth relationship: $V = 2000 + 0.8 Z$ (m/s).

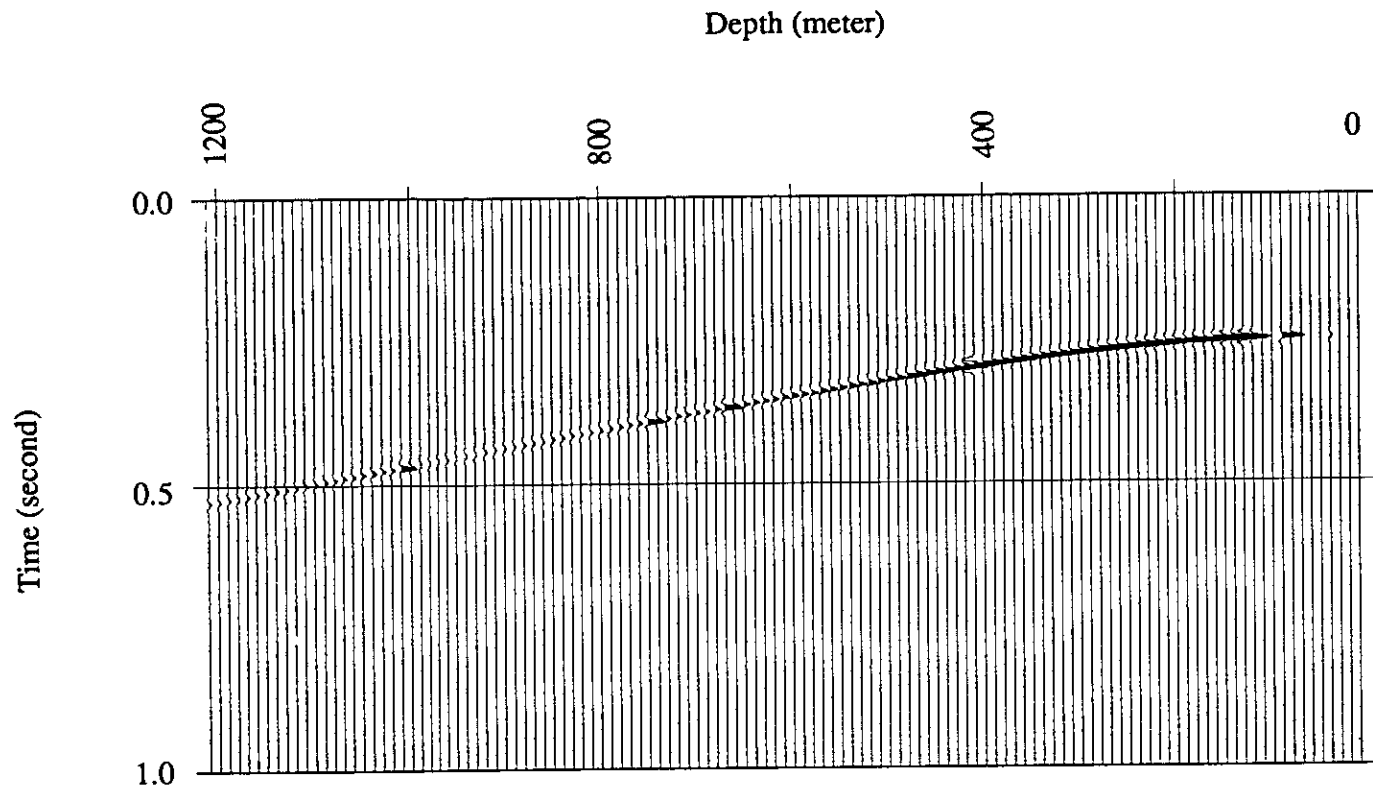


FIG. 3. Synthetic crosswell shot gather for source depth = 0 m. (Only direct arrival is shown here.)

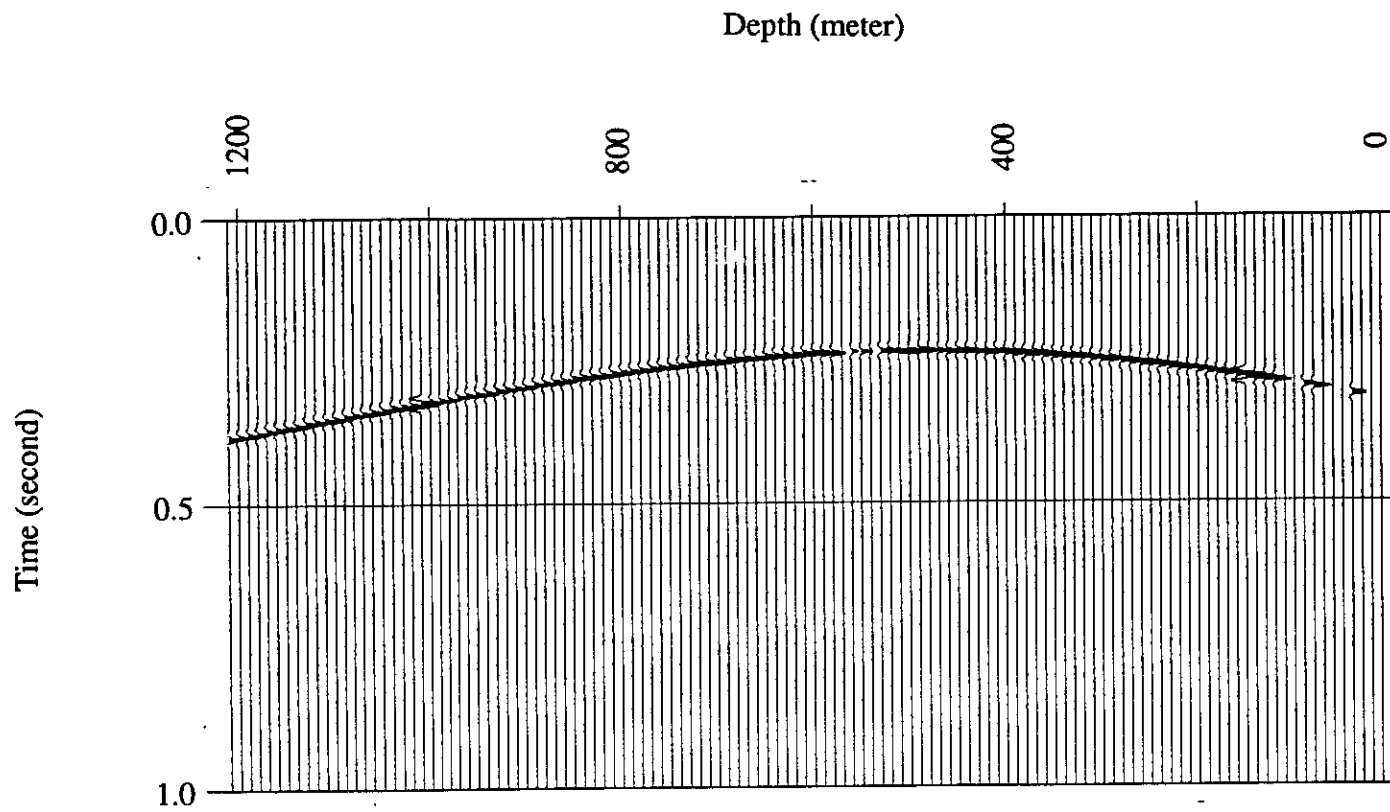
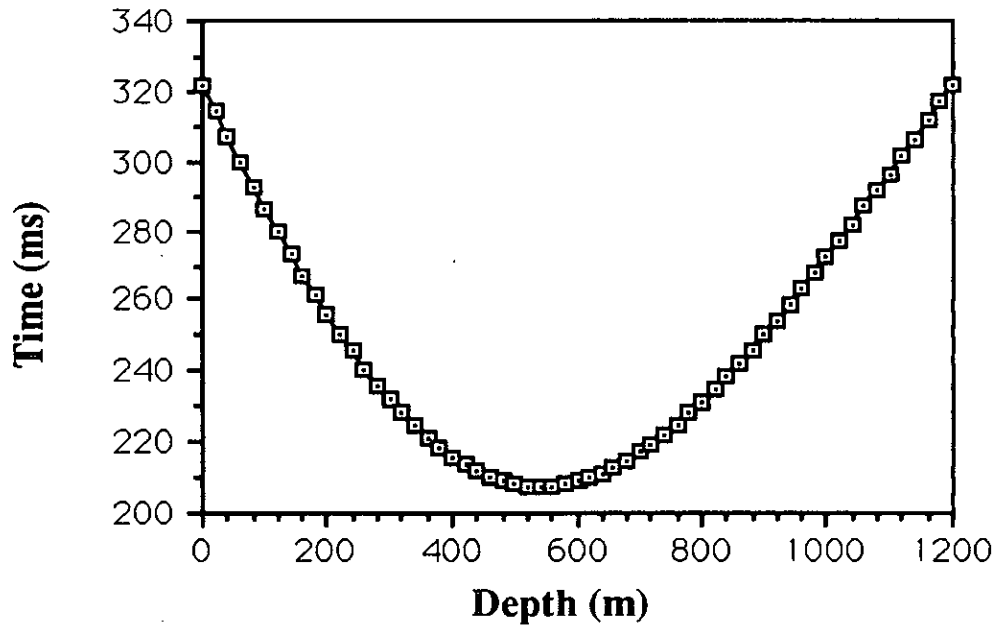
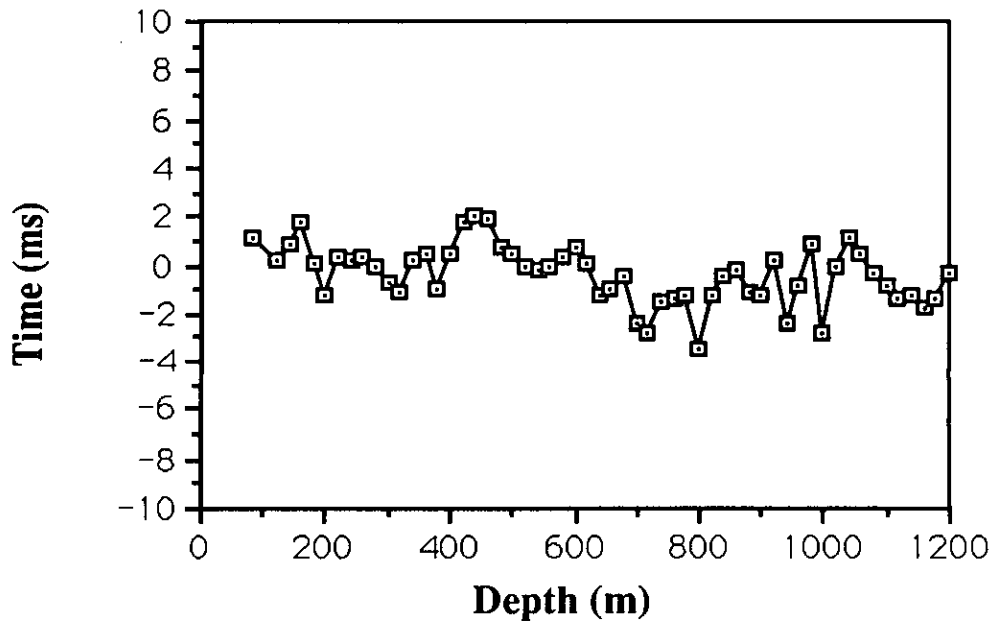


FIG. 4. Synthetic crosswell shot gather for source depth = 500 m. (Only direct arrival is shown here.)



(a) Theoretical traveltime curve



(b) Differential traveltime

FIG. 5. Theoretically calculated traveltimes (a) and comparison with observed traveltimes from synthetic crosswell shot gather (b) (source depth = 500 m).

CONTOUR MAP FOR SEMBLANCE VALUES

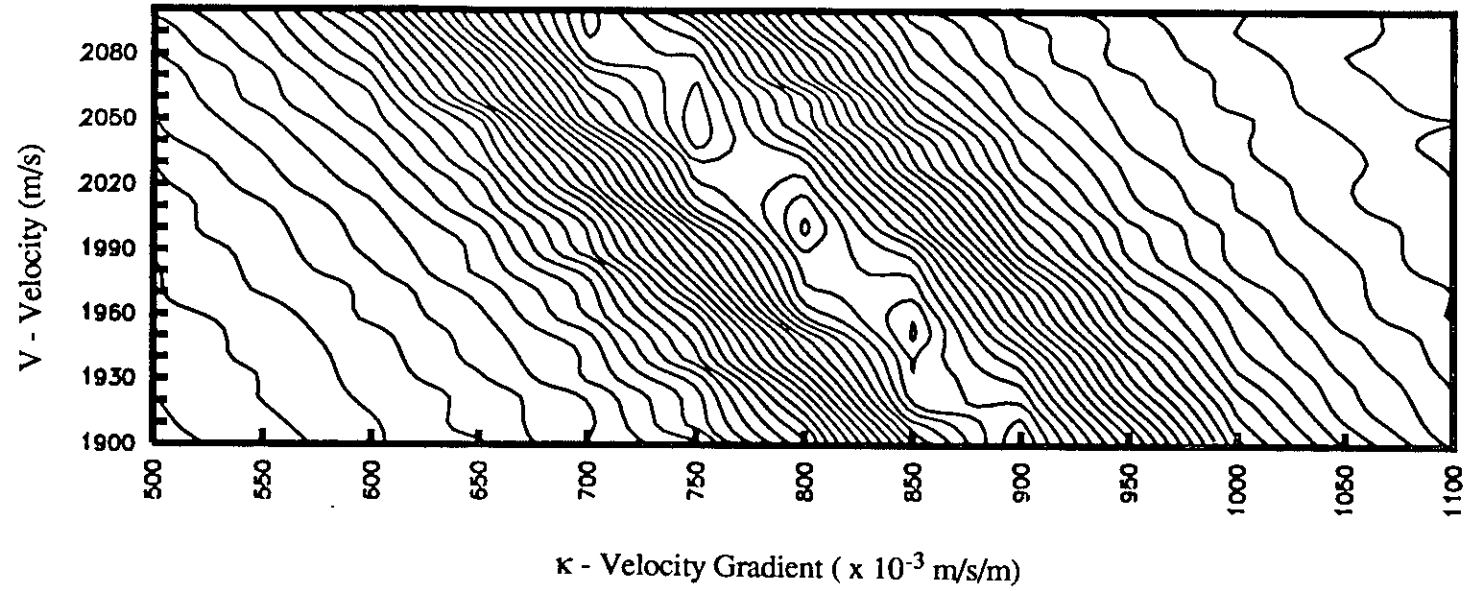


FIG. 6. Result of semblance analysis for synthetic crosswell common-shot gather (source depth = 0m). The maximum semblance value appears where $V = 2000$ m/s and $\kappa = 0.8$ m/s/m.

CONTOUR MAP FOR SEMBLANCE VALUES

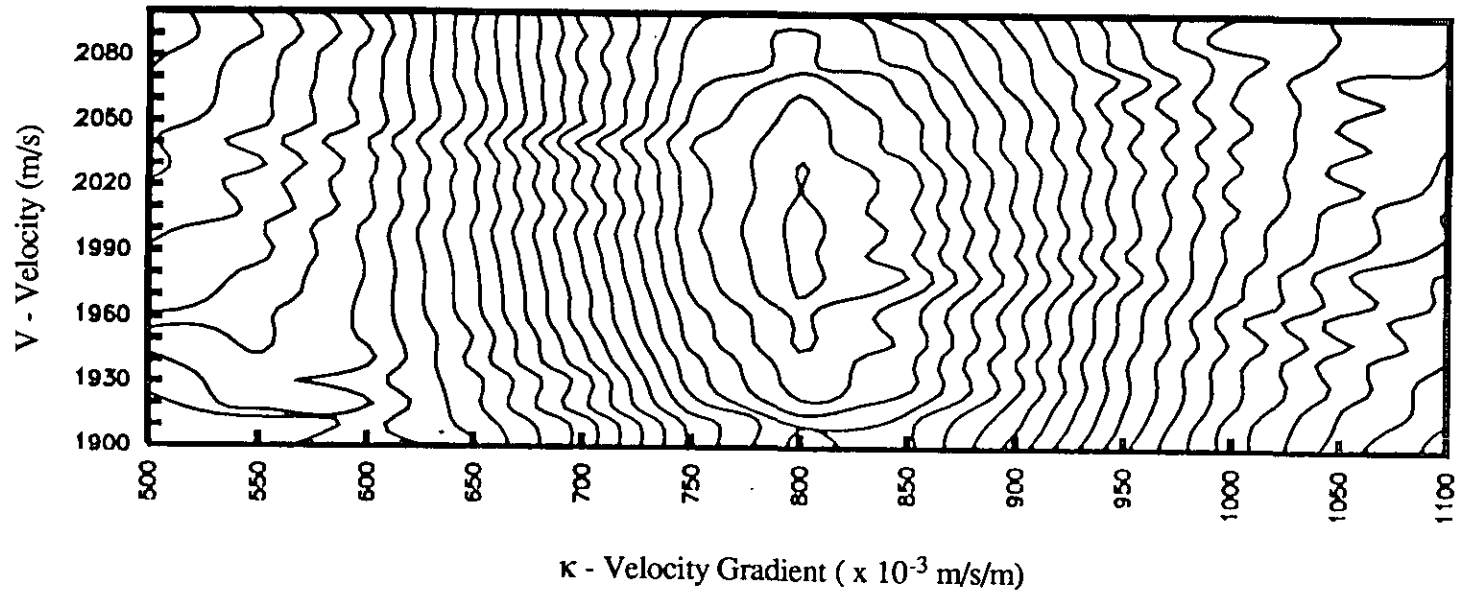


FIG. 7. Result of semblance analysis for synthetic crosswell common-shot gather (source depth = 500m). The maximum semblance value appears where $V = 2000$ m/s and $\kappa = 0.8$ m/s/m.

CONTOUR MAP FOR SEMBLANCE VALUES

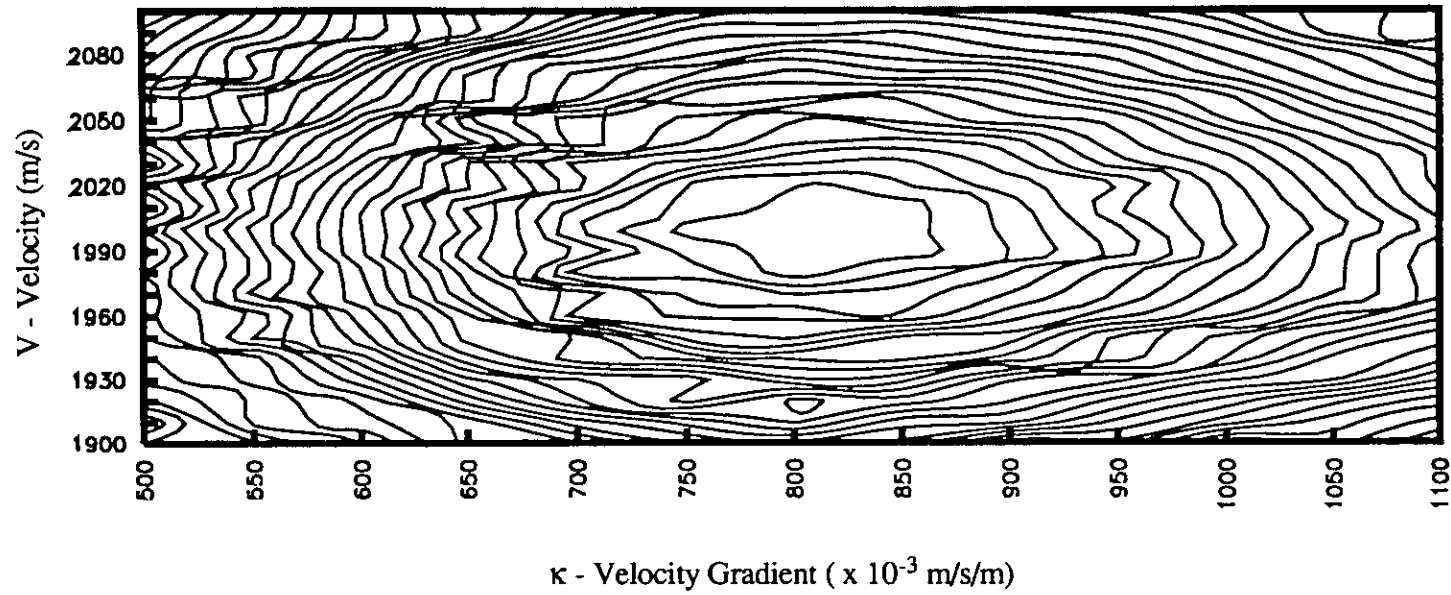


FIG. 8. Result of semblance analysis for synthetic crosswell common-shot gather (source depth = 760m). The maximum semblance value appears where $V = 2000$ m/s and $\kappa = 0.8$ m/s/m.

CONTOUR MAP FOR SEMBLANCE VALUES

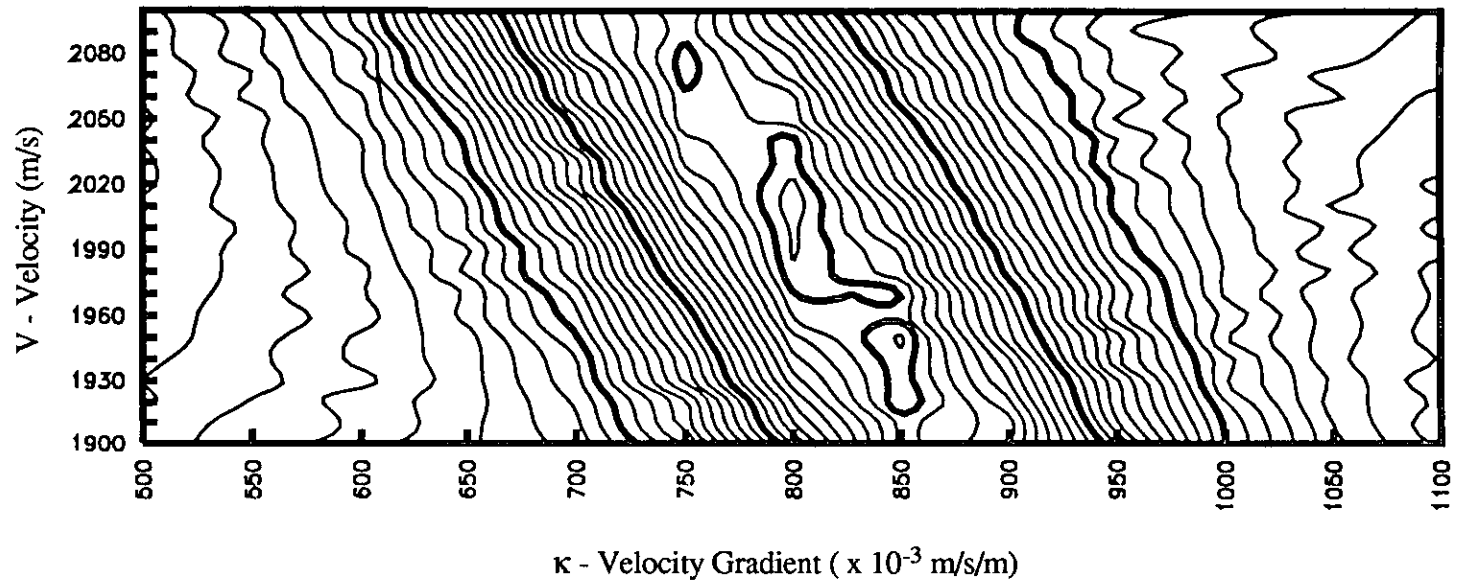


FIG. 9. Result of semblance analysis for synthetic crosswell common-shot gather (source depth = 260m). The maximum semblance value appears where $V = 2010$ m/s and $\kappa = 0.8$ m/s/m.

CONTOUR MAP FOR SEMBLANCE VALUES

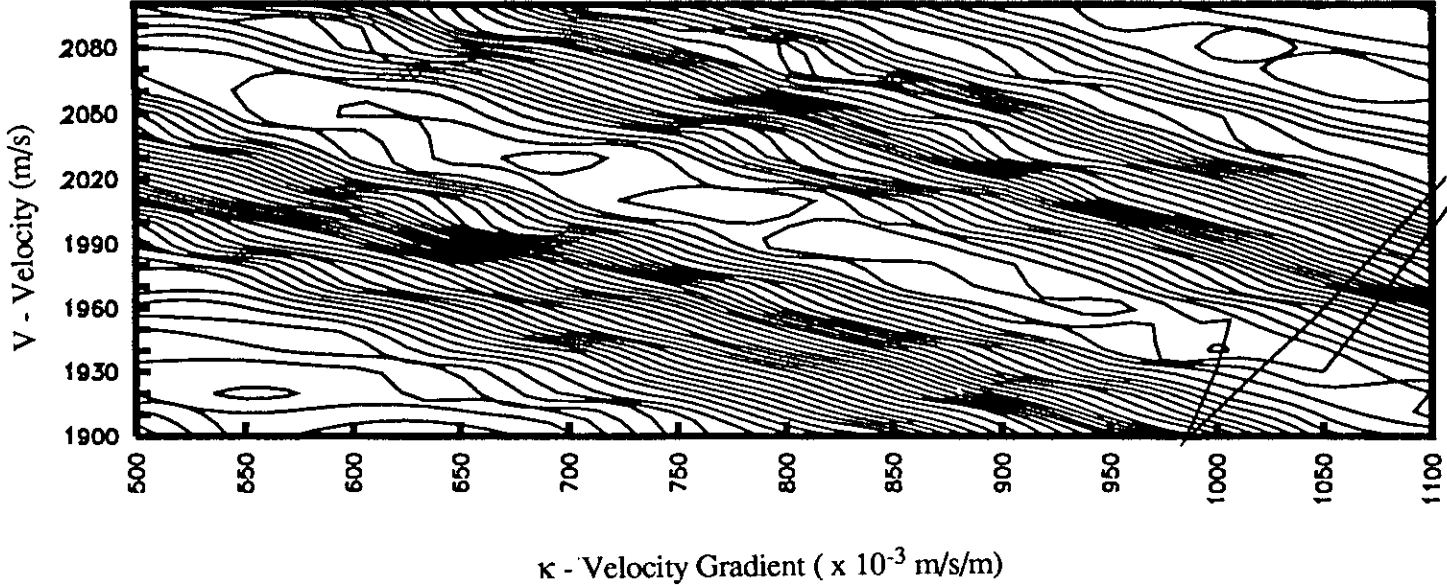


FIG. 10. Result of semblance analysis for synthetic crosswell common-shot gather (source depth = 1000m). The maximum semblance value appears where V = 1990 m/s and $\kappa = 0.825$ m/s/m.

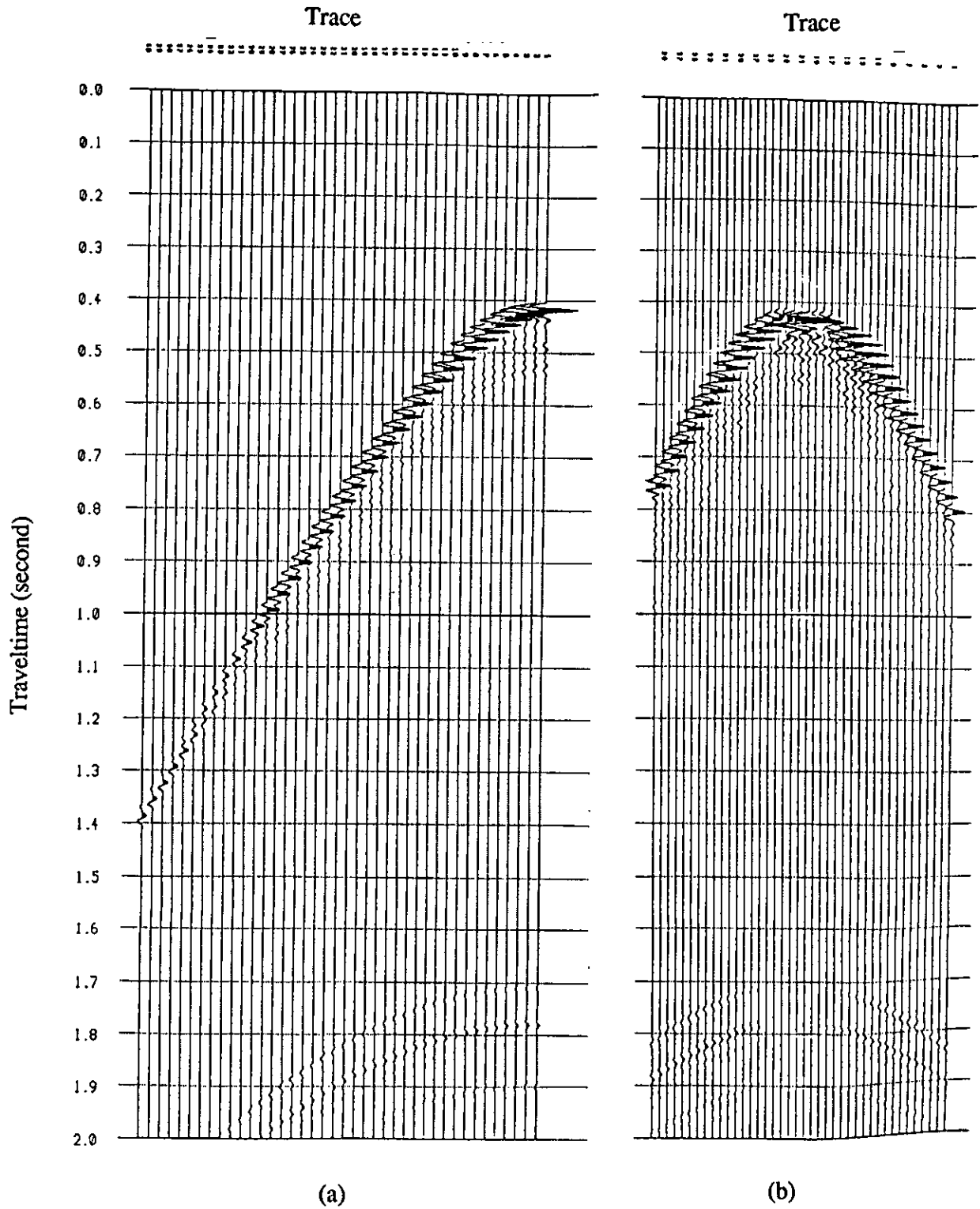


FIG. 11. Shot records from an ultrasonic seismic modeling experiment in a water tank (Stewart and Cheadle, 1989). (a) Source depth = 0 m; and (b) Source depth = 1000 m.

CONTOUR MAP FOR SEMBLANCE VALUES

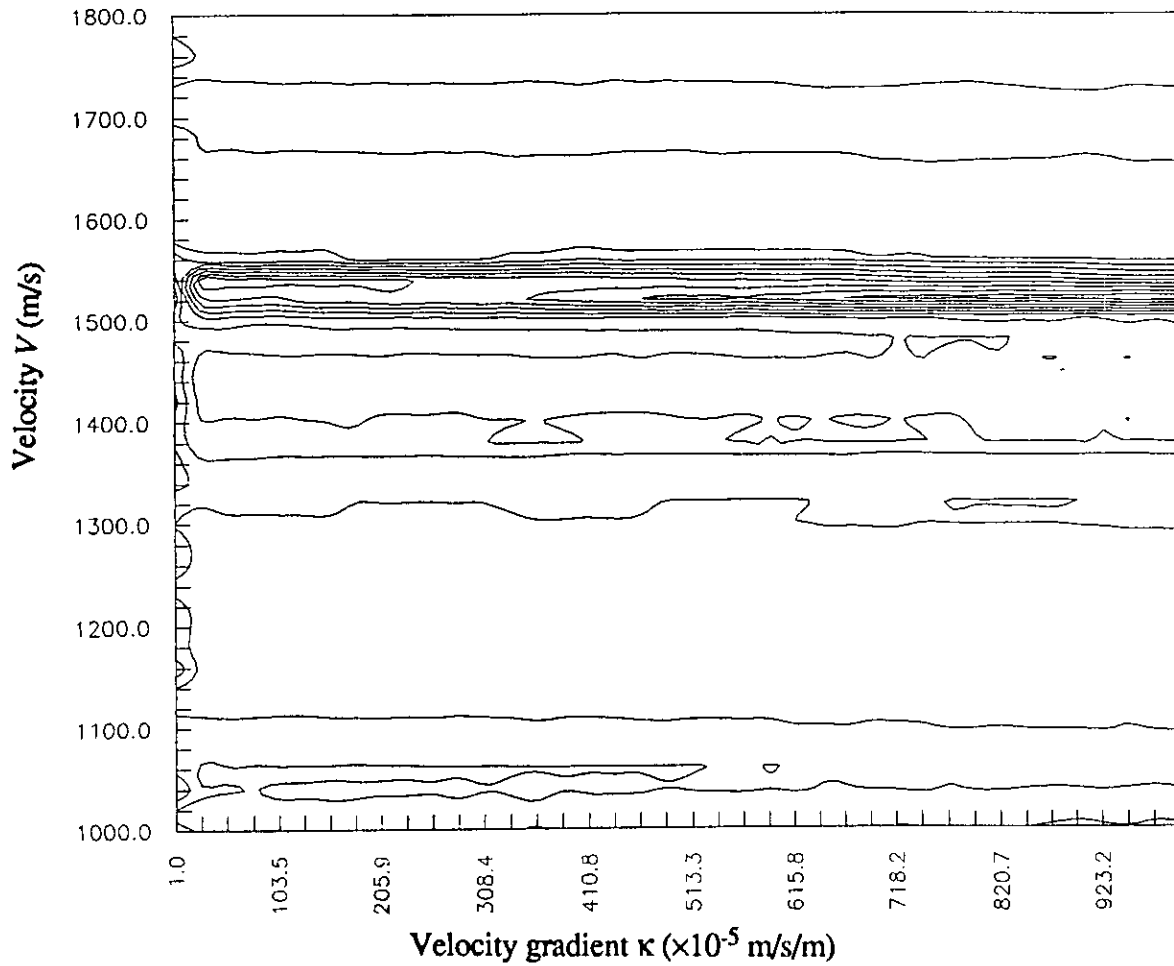


FIG. 12. Result of semblance analysis for physical modeling crosswell common-shot gather (source depth = 0 m). The largest semblance value appears where $V = 1520$ m/s and $\kappa = 0.0095$ m/s/m.

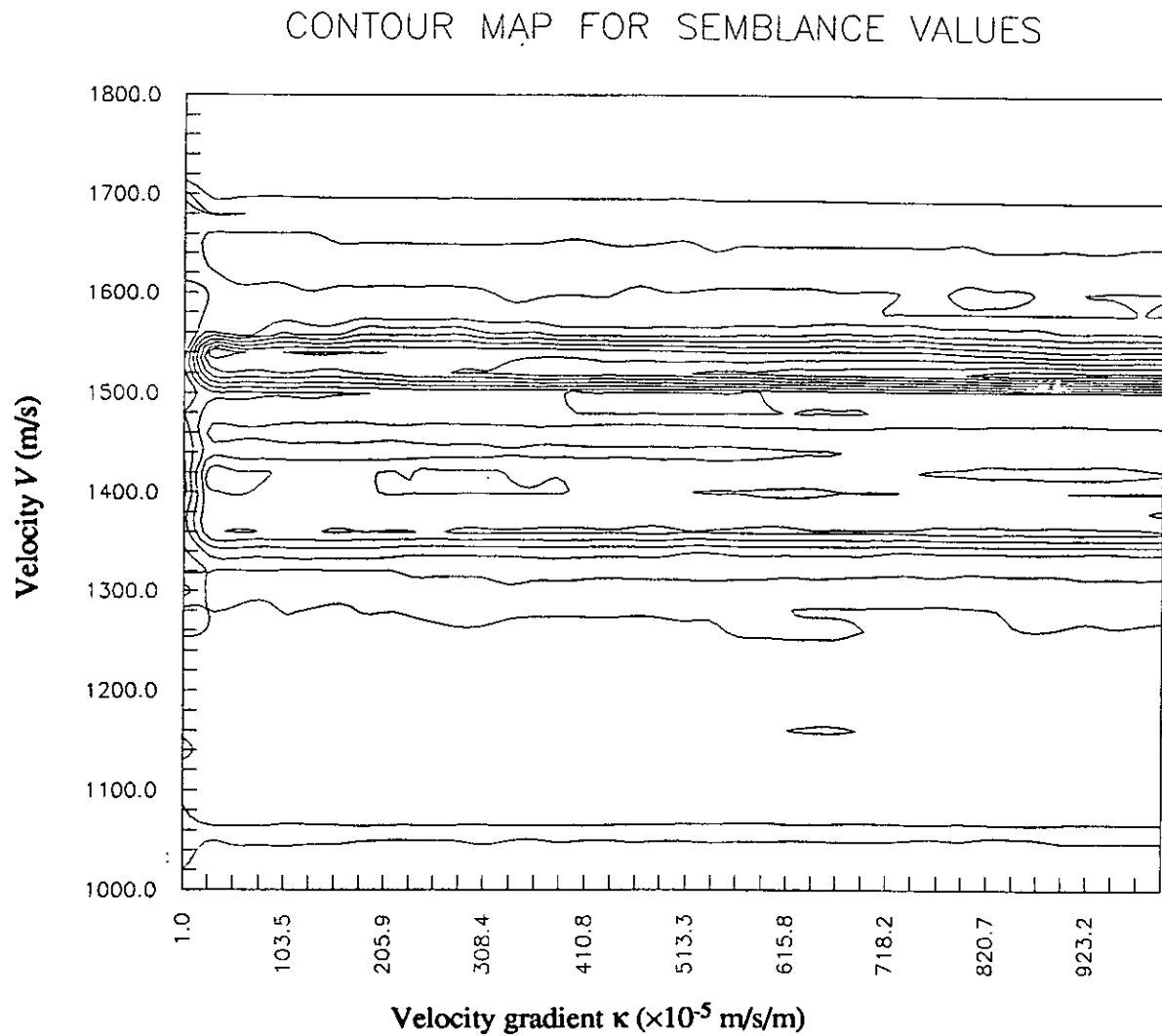


FIG. 13. Result of semblance analysis for physical modeling crosswell common-shot gather (source depth = 450 m). The largest semblance value appears where $V = 1520$ m/s and $\kappa = 0.0085$ m/s/m.

CONTOUR MAP FOR SEMBLANCE VALUES

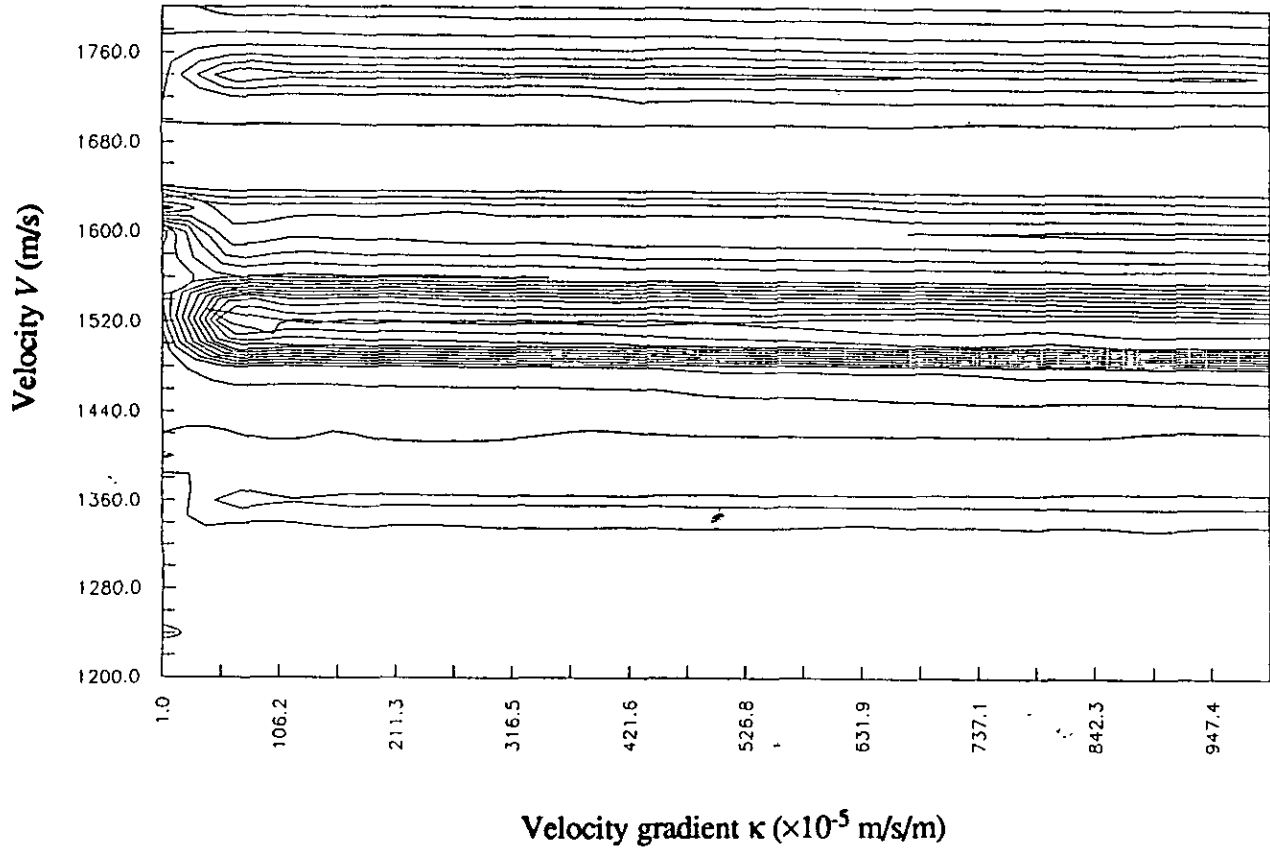


FIG. 14. Result of semblance analysis for physical modeling crosswell common-shot gather (source depth = 1000 m). The largest semblance value appears where $V = 1520$ m/s and $\kappa = 0.0065$ m/s/m.

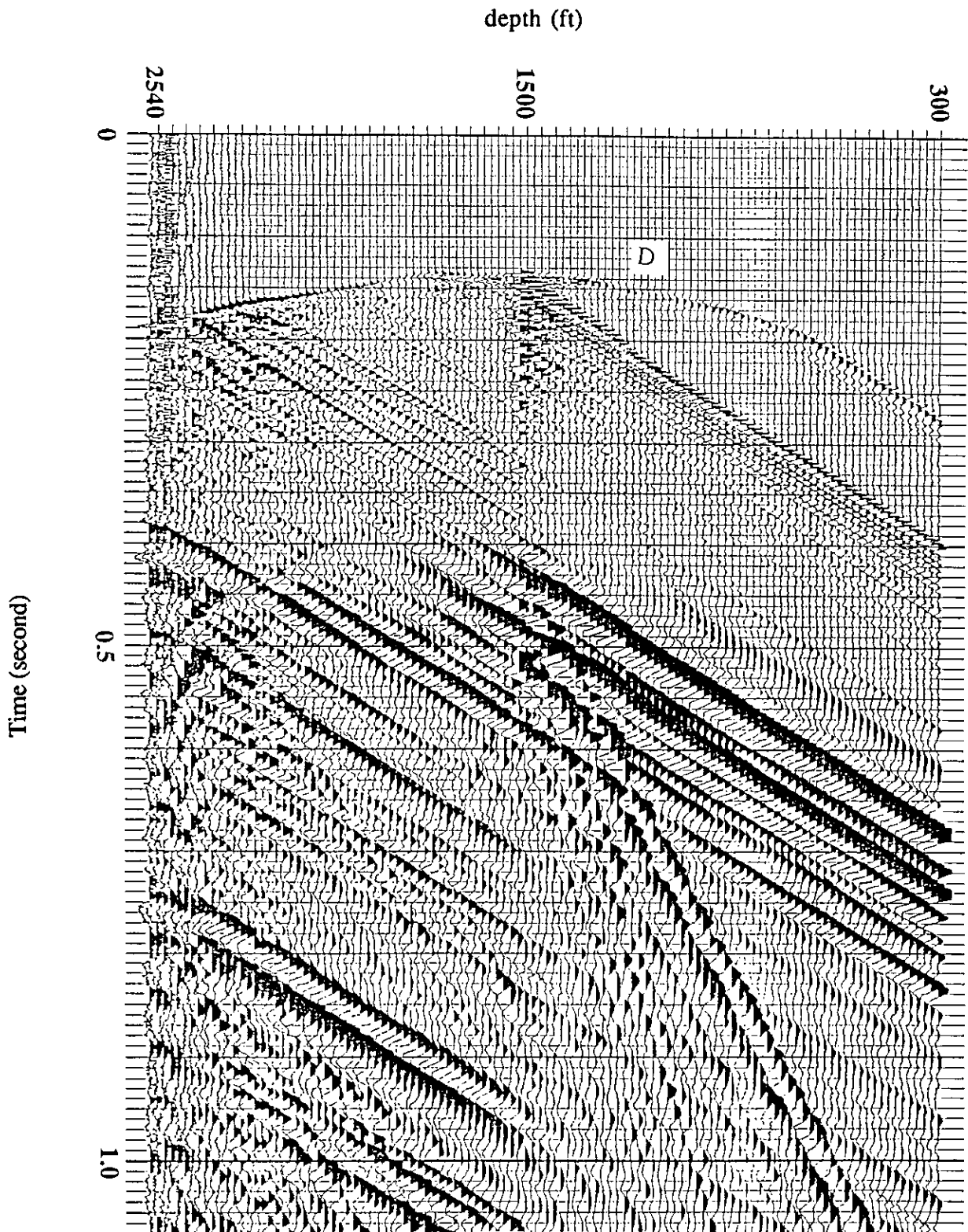


FIG. 15. Common-receiver gather of crosswell seismic data acquired in Humble, Texas. Source depths range from 300 ft to 2540 ft at interval of 20 ft. The geophone is located at 1500 ft. Offset between wells is 815 ft. *D* represents P-wave direct arrivals. (Courtesy by Texaco Inc.)

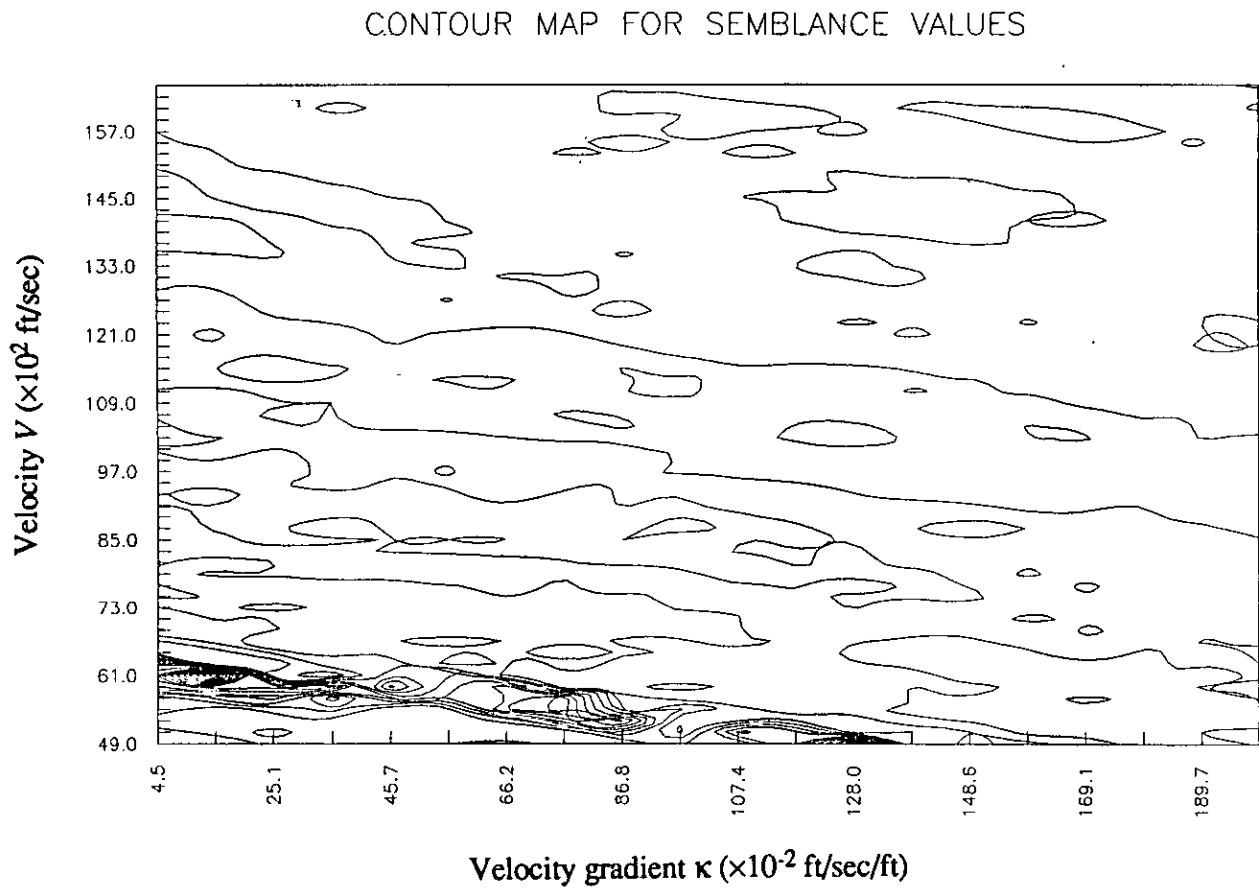


FIG. 16. Result of semblance analysis for real crosswell seismic data shown in Figure 15. Initial velocity of 6100 ft/sec and velocity gradient of 0.145 ft/sec/ft are picked at the point with the largest semblance value.